Inorg. Chem. **2004**, *43*, 1082–1089

Syntheses, Structure, and Selected Physical Properties of $CsLnMnSe_3$ (Ln = Sm, Gd, Tb, Dy, Ho, Er, Tm, Yb, Y) and $AYbZnQ_3$ (A = Rb, Cs; Q = S, Se, Te)

Kwasi Mitchell,[†] Fu Qiang Huang,[†] El'ad N. Caspi,[‡] Adam D. McFarland,[†] Christy L. Haynes,[†] Rebecca C. Somers,[†] James D. Jorgensen,[‡] Richard P. Van Duyne,[†] and James A. Ibers*,[†]

Department of Chemistry, Northwestern University, 2145 Sheridan Road, Evanston, Illinois 60208, and Materials Science Division, Argonne National Laboratory, Argonne, Illinois 60439

Received July 21, 2003

$CsLnMnSe_3$ (Ln = Sm, Gd, Tb, Dy, Ho, Er, Tm, Yb, Y) and $AYbZnQ_3$ (A = Rb, Cs; Q = S, Se, Te) have been synthesized from solid-state reactions at temperatures in excess 1173 K. These isostructural materials crystallize in the layered $KZrCuS_3$ structure type in the orthorhombic space group *Cmcm*. The structure is composed of LnQ_6 octahedra and MQ_4 tetrahedra that share edges to form $^2_\infty[LnMQ_3]$ layers. These layers stack perpendicular to [010] and are separated by layers of face- and edge-sharing AQ_8 bicapped trigonal prisms. There are no Q–Q bonds in the structure of the $ALnMQ_3$ compounds so the formal oxidation states of A/Ln/M/Q are 1+/3+/2+/2–. The $CsLnMnSe_3$ materials, with the exception of $CsYbMnSe_3$, are Curie–Weiss paramagnets between 5 and 300 K. The magnetic susceptibility data for $CsYbZnS_3$, $RbYbZnSe_3$, and $CsYbMSe_3$ (M = Mn, Zn) show a weak cusp at approximately 10 K and pronounced differences between field-cooled and zero-field-cooled data. However, $CsYbZnSe_3$ is not an antiferromagnet because a neutron diffraction study indicates that $CsYbZnSe_3$ shows neither long-range magnetic ordering nor a phase change between 4 and 295 K. Nor is the compound a spin glass because the transition at 10 K does not depend on ac frequency. The optical band gaps of the (010) and (001) crystal faces for $CsYbMnSe_3$ are 1.60 and 1.59 eV, respectively; the optical band of the (010) crystal faces for $CsYbZnS_3$ and $RbYbZnSe_3$ are 2.61 and 2.07 eV, respectively.

Introduction

The number of new alkali-metal or alkaline-earth/rare-earth/transition-metal/chalcogenides (A/Ln/M/Q) has increased dramatically over the past decade owing to the utility of the reactive-flux technique.[1] The low melting points of the A_xQ_y fluxes (433−723 K) and their ability to act as both reagent and reaction medium have led to the isolation of kinetic species that cannot be obtained by the use of traditional high-temperature solid-state experimental methods. Although this technique more readily produces kinetic species, crystal growth remains a challenge and multiple products may be stabilized. This has limited the physical characterization of a number of materials. However, the use of reactive alkali-metal fluxes has proven to be invaluable in the synthesis of a host of low-dimensional phases with interesting structures.[2] Most of the compounds synthesized contain a coinage metal (Cu, Ag, or Au) as the d-element and thus show similar physical properties. Most of the compounds characterized are semiconductors; exceptions are the metals $KCeCuTe_4$[3] and $KEuCu_2Te_4$.[4] No long-range magnetic transitions have been found in the A/Ln/M/Q materials.

There are few known A/Ln/M/Q materials, where M ≠ Cu, Ag, or Au, despite the fact that such compounds can exhibit interesting physical properties, for example the magnetic properties of the $BaLn_2MS_5$ (Ln = La−Nd, M = Mn−Co, Zn) materials.[5−11] Moreover, there are few consistent studies of A/Ln/M/Q materials across both the Ln and

* To whom correspondence should be addressed. E-mail: ibers@chem.northwestern.edu.
[†] Northwestern University.
[‡] Argonne National Laboratory.

(1) Sunshine, S. A.; Kang, D.; Ibers, J. A. *J. Am. Chem. Soc.* **1987**, *109*, 6202−6204.
(2) Mitchell, K.; Ibers, J. A. *Chem. Rev.* **2002**, *102*, 1929−1952.
(3) Patschke, R.; Heising, J.; Kanatzidis, M. *Chem. Mater.* **1998**, *10*, 695−697.
(4) Patschke, R.; Brazis, P.; Kannewurf, C. R.; Kanatzidis, M. G. *J. Mater. Chem.* **1999**, *9*, 2293−2296.
(5) Masuda, H.; Fujino, T.; Sato, N.; Yamada, K. *J. Solid State Chem.* **1999**, *146*, 336−343.

10.1021/ic030232+ CCC: $27.50
Published on Web 01/06/2004

Table 1. $CsLnMSe_3$ Compounds Synthesized and Structurally Characterized[a]

	La	Ce	Pr	Nd	Sm	Eu	Gd	Tb	Dy	Y	Ho	Er	Tm	Yb
Mn					X[b]		X	X	X	X	X	X	X	X
Zn[c]					X		X	X	X	X	X	X	X	X
Cd[d]	∇	X	X	∇	X		X	X	X	X				
Hg[d]	X	X	X	X	X		X	∇	∇	X				

[a] Also synthesized and structurally characterized were $CsYbZnS_3$, $RbYbZnSe_3$, $RbYbZnTe_3$, and $CsYbZnTe_3$. [b] An "X" indicates the compound was characterized by single-crystal X-ray diffraction techniques, a "∇" indicates the compound was characterized by EDX measurements only, and a blank indicates that the attempted synthesis was unsuccessful. [c] Information taken from ref 12. [d] Information taken from ref 13.

M series for a given structure type. This is indeed a major oversight since such studies are essential if correlations between structural and physical properties are to be drawn. This paper details the syntheses, structure, and selected physical properties of the $CsLnMnSe_3$ (Ln = Sm, Gd, Tb, Dy, Ho, Er, Tm, Yb, Y) and $AYbZnQ_3$ (A = Rb, Cs; Q = S, Se, Te) materials. These compounds, which are extensions of the previously characterized $CsLnMSe_3$ (M = Zn, Cd, Hg) compounds,[12,13] were synthesized with the use of the reactive-flux technique. These materials crystallize in the layered $KZrCuS_3$ structure type.[14] This is the simplest and the most prevalent structure among the A/Ln/M/Q materials, facilitating the assessment of the effects of chemical substitution on the magnetic and optical properties of the compounds. Our previous investigation of the $CsLnMSe_3$ compounds demonstrated their interesting optical properties. This investigation details how the optical and magnetic properties of the $ALnMQ_3$ materials vary with further chemical substitutions.

For convenience, in Table 1 we tabulate those $ALnMQ_3$ compounds whose crystal structures we have determined.

Experimental Section

Syntheses. The following reagents were used as obtained: Rb (Strem, 99.9%), Cs (Aldrich, 99.5%), Sm (Alfa Aesar, 99.9%), Gd (Strem, 99.9%), Tb (Alfa Aesar, 99.9%), Dy (Alfa Aesar, 99.9%), Ho (Alfa Aesar, 99.9%), Er (Strem, 99.9%), Tm (Strem, 99.9%), Yb (Strem, 99.9%), Y (Alfa Aesar, 99.9%), Mn (Alfa Aesar, 99.9%), Zn (Johnson Matthey, 99.99%), S (Alfa Aesar, 99.99%), Se (Cerac, 99.99%), Te (Aldrich, 99.8%), RbI (Strem, 99%), and CsI (Aldrich, 99.99%). The reactive fluxes employed in the syntheses, namely Cs_2S_3, Cs_2Se_3, Cs_2Te_3, Rb_2Se_3, and Rb_2Te_3, were prepared by the stoichiometric reactions of the elements in liquid NH_3. Reaction mixtures were loaded into carbon-coated fused-silica tubes in an Ar filled glovebox. These tubes were sealed under a 10^{-4} Torr atmosphere and then placed in a computer-controlled furnace. After heating, the reaction mixtures were washed with water, and then with *N*,*N*-dimethylformamide, and finally the mixtures were dried with acetone. The products of these reactions, as determined by the examination of selected single crystals with an EDX-equipped Hitachi S-3500 SEM, were consistent with the stated compositions. Several of the compounds are air sensitive, exhibiting signs of surface decomposition after being exposed to the atmosphere for several hours.

$CsYbZnSe_3$. The synthesis of $CsYbZnSe_3$ was detailed earlier.[12]

$CsLnMnSe_3$ (Ln = Sm, Gd, Tb, Dy, Ho, Er, Tm, Yb, Y). Reaction mixtures consisted of 0.3 mmol of Cs_2Se_3, 0.5 of mmol Ln, 0.5 mmol of Mn, 1.0 mmol of Se, and approximately 150 mg of CsI (used to aid crystal growth). The samples were heated to 1273 K in 48 h, kept at 1273 K for 50 h, cooled at 4 K/h to 473 K, and then the furnace was turned off. The desired $CsLnMnSe_3$ product, which consisted of red-brown plates and needles, was obtained in 85−95% yield, based upon Ln. In a few instances the desired product was contaminated with MnSe and unidentified ternary phases (Cs/Ln/Se).

$CsYbZnS_3$ and $RbYbZnSe_3$. Reaction mixtures consisted of 0.3 mmol of Cs_2S_3 or Rb_2Se_3, 0.5 mmol of Yb, 0.5 mmol of Zn, 1.0 mmol of S or Se, and approximately 150 mg of CsI or RbI. The samples were heated to 1173 K in 48 h, kept at 1173 K for 96 h, and cooled to room temperature in 148 h. $CsYbZnS_3$ and $RbYbZnSe_3$ crystallized as yellow and red needles, respectively, in approximately 80% yield, based upon Ln. Side products of the reactions were Yb/Q and ZnQ binary compounds.

$RbYbZnTe_3$ and $CsYbZnTe_3$. Reaction mixtures of 0.3 mmol of Rb_2Te_3 or Cs_2Te_3, 0.5 mmol of Yb, 0.5 mmol of Zn, 1.0 mmol of Te, and approximately 200 mg of RbI or CsI were heated to 1173 K in 24 h, kept at 1173 K for 96 h, cooled to 473 K in 120 h, and then rapidly cooled to room temperature. Only a few black needles of $RbYbZnTe_3$ and $CsYbZnTe_3$ were obtained from the reactions.

Structure Determinations. Structural data for $CsYbZnSe_3$ were reported previously.[12] For the present $ALnMQ_3$ materials, single-crystal X-ray diffraction data were collected with the use of graphite-monochromatized Mo Kα radiation (λ = 0.71073 Å) at 153 K on a Bruker Smart-1000 CCD diffractometer.[15] The crystal-to-detector distance was 5.023 cm. Crystal decay was monitored by re-collecting 50 initial frames at the end of data collection. Data were collected by a scan of 0.3° in ω in three groups of 606 frames at φ settings of 0°, 120°, and 240° for $CsTmMnSe_3$, $CsYbZnS_3$, and $RbYbZnTe_3$ and in four groups of 606 frames at φ settings of 0°, 90°, 180°, and 270° for the remaining compounds. The exposure times varied from 10 to 25 s/frame. The collection of the intensity data was carried out with the program SMART.[15] Cell refinement and data reduction were carried out with the use of the program SAINT,[15] and face-indexed absorption corrections were performed numerically with the use of the program XPREP.[16] Then the program SADABS[15] was employed to make incident beam and decay corrections.

The structures were solved with the direct methods program SHELXS and refined with the full-matrix least-squares program

(6) Wakeshima, M.; Hinatsu, Y. *J. Solid State Chem.* **2000**, *153*, 330−335.
(7) Wakeshima, M.; Hinatsu, Y.; Oikawa, K.; Shimojo, Y.; Morii, Y. *J. Mater. Chem.* **2000**, *10*, 2183−2185.
(8) Wakeshima, M.; Hinatsu, Y. *J. Solid State Chem.* **2001**, *159*, 163−169.
(9) Ino, K.; Wakeshima, M.; Hinatsu, Y. *Mater. Res. Bull.* **2001**, *36*, 2207−2213.
(10) Wakeshima, M.; Hinatsu, Y.; Ishii, Y.; Shimojo, Y.; Morii, Y. *J. Mater. Chem.* **2002**, *12*, 631−634.
(11) Koo, H.-J.; Whangbo, M.-H.; Lee, K.-S. *J. Solid State Chem.* **2002**, *169*, 143−148.
(12) Mitchell, K.; Haynes, C. L.; McFarland, A. D.; Van Duyne, R. P.; Ibers, J. A. *Inorg. Chem.* **2002**, *41*, 1199−1204.
(13) Mitchell, K.; Huang, F. Q.; McFarland, A. D.; Haynes, C. L.; Somers, R. C.; Van Duyne, R. P.; Ibers, J. A. *Inorg. Chem.* **2003**, *42*, 4109−4116.
(14) Mansuetto, M. F.; Keane, P. M.; Ibers, J. A. *J. Solid State Chem.* **1992**, *101*, 257−264.
(15) *SMART Version 5.054 Data Collection and SAINT-Plus Version 6.22 Data Processing Software for the SMART System*; Bruker Analytical X-ray Instruments, Inc.: Madison, WI, 2000.
(16) Sheldrick, G. M. *SHELXTL DOS/Windows/NT Version 6.12*; Bruker Analytical X-ray Instruments, Inc.: Madison, WI, 2000.

Table 2. Crystal Data and Structure Refinements for $CsLnMnSe_3$[a]

	$CsSmMnSe_3$	$CsGdMnSe_3$	$CsTbMnSe_3$	$CsDyMnSe_3$	$CsHoMnSe_3$	$CsErMnSe_3$	$CsTmMnSe_3$	$CsYbMnSe_3$	$CsYMnSe_3$
fw	575.08	581.98	583.65	587.23	589.66	591.99	593.66	597.77	513.64
a, Å	4.2618(7)	4.2355(8)	4.2158(3)	4.1984(4)	4.1899(8)	4.1736(4)	4.1616(5)	4.1447(8)	4.1978(4)
b, Å	15.715(3)	15.761(3)	15.767(1)	15.773(1)	15.799(3)	15.804(2)	15.808(2)	15.787(3)	15.796(1)
c, Å	11.223(2)	11.138(2)	11.0861(9)	11.050(1)	11.017(2)	10.969(1)	10.948(1)	10.932(2)	11.040(1)
V, Å^3	751.7(2)	743.5(2)	736.9(1)	731.7(1)	729.3(2)	723.5(1)	720.2(2)	715.3(2)	732.1(1)
ρ_c, g cm^{-3}	5.082	5.199	5.261	5.330	5.371	5.435	5.475	5.551	4.660
μ, cm^{-1}	285.92	299.28	307.95	315.58	322.68	331.88	340.06	349.12	293.03
$R(F)$[b]	0.0177	0.0186	0.0147	0.0161	0.0191	0.0181	0.0198	0.0175	0.0187
$R_w(F^2)$[c]	0.0486	0.0498	0.0471	0.0589	0.0568	0.0591	0.0552	0.0552	0.0575

[a] For all structures, $Z = 4$, space group = *Cmcm*, $T = 153(2)$ K, and $\lambda = 0.71073$ Å. [b] $R(F) = \sum||F_o| - |F_c||/\sum|F_o|$ for $F_o^2 > 2\sigma(F_o^2)$. [c] $R_w(F^2) = \{\sum w(F_o^2 - F_c^2)^2/\sum wF_o^4\}^{1/2}$ for all data. $w^{-1} = \sigma^2(F_o^2) + (q \times F_o^2)^2$ for $F_o^2 \geq 0$ and $w^{-1} = \sigma^2(F_o^2)$ for $F_o^2 < 0$. $q = 0.02$ for Ln = Tb; otherwise, $q = 0.04$.

Table 3. Selected Bond Lengths (Å) for $CsLnMnSe_3$

	$CsSmMnSe_3$	$CsGdMnSe_3$	$CsTbMnSe_3$	$CsDyMnSe_3$	$CsHoMnSe_3$	$CsErMnSe_3$	$CsTmMnSe_3$	$CsYbMnSe_3$	$CsYMnSe_3$
Cs−Se1 × 4	3.7470(5)	3.7480(6)	3.7496(5)	3.7506(5)	3.7534(7)	3.7513(5)	3.7529(5)	3.7504(6)	3.7535(4)
Cs−Se1 × 2	3.9283(7)	3.8941(7)	3.8727(5)	3.8606(5)	3.8469(8)	3.8291(6)	3.8225(6)	3.8173(8)	3.8553(5)
Cs−Se2 × 2	3.6132(7)	3.6142(8)	3.6082(7)	3.6033(6)	3.6078(9)	3.6047(7)	3.6015(7)	3.5926(8)	3.6109(6)
Ln-Se1 × 4	2.9206(4)	2.9058(5)	2.8896(3)	2.8763(4)	2.8710(5)	2.8604(4)	2.8498(4)	2.8360(5)	2.8773(3)
Ln-Se2 × 2	2.9325(5)	2.9121(5)	2.9009(3)	2.8928(3)	2.8845(6)	2.8729(3)	2.8690(4)	2.8659(5)	2.8893(3)
Mn−Se1 × 2	2.5084(6)	2.5043(7)	2.5061(7)	2.5043(6)	2.5027(8)	2.5000(7)	2.5008(7)	2.4996(8)	2.5030(6)
Mn−Se2 × 2	2.5898(7)	2.5860(8)	2.5788(7)	2.5714(7)	2.5725(8)	2.5663(8)	2.5623(8)	2.5550(8)	2.5749(7)
Ln···Mn	3.5773(5)	3.5649(5)	3.5384(3)	3.5258(3)	3.5185(5)	3.5043(3)	3.4964(4)	3.4874(5)	3.5256(3)

Table 4. Crystal Data and Structure Refinements for $AYbZnQ_3$[a]

	$CsYbZnS_3$	$RbYbZnSe_3$	$RbYbZnTe_3$	$CsYbZnTe_3$
fw	467.50	560.76	706.68	754.12
a, Å	3.9543(5)	4.0737(4)	4.3228(5)	4.3377(6)
b, Å	15.276(2)	15.066(2)	15.970(2)	16.704(2)
c, Å	10.440(1)	10.788(1)	11.480(1)	11.509(2)
V, Å^3	630.6(1)	662.1(1)	792.5(2)	833.9(2)
ρ_c, g cm^{-3}	4.924	5.626	5.923	6.007
μ, cm^{-1}	250.79	413.17	315.64	285.02
$R(F)$[b]	0.0205	0.0151	0.0244	0.0323
$R_w(F^2)$[c]	0.0494	0.0430	0.0634	0.0674

[a] For all structures, $Z = 4$, space group = *Cmcm*, $T = 153(2)$ K, and $\lambda = 0.71073$ Å. [b] $R(F) = \sum||F_o| - |F_c||/\sum|F_o|$ for $F_o^2 > 2\sigma(F_o^2)$. [c] $R_w(F^2) = \{\sum w(F_o^2 - F_c^2)^2/\sum wF_o^4\}^{1/2}$ for all data. $w^{-1} = \sigma^2(F_o^2) + (q \times F_o^2)^2$ for $F_o^2 \geq 0$ and $w^{-1} = \sigma^2(F_o^2)$ for $F_o^2 < 0$. $q = 0.02$ for $CsYbZnS_3$ and $RbYbZnSe_3$; $q = 0.037$ for $RbYbZnTe_3$; and $q = 0.036$ for $CsYbZnTe_3$.

Table 5. Selected Bond Lengths (Å) for $AYbZnQ_3$

	$CsYbZnS_3$	$RbYbZnSe_3$	$RbYbZnTe_3$	$CsYbZnTe_3$
A−Q1 × 4	3.608(1)	3.5410(6)	3.6977(8)	3.8425(9)
A−Q1 × 2	3.726(2)	3.7833(6)	4.0116(9)	4.066(1)
A−Q2 × 2	3.486(2)	3.4299(8)	3.636(1)	3.790(1)
Yb−Q1 × 4	2.7017(9)	2.8177(4)	3.0264(4)	3.0328(6)
Yb−Q2 × 2	2.7237(6)	2.8464(3)	3.0501(4)	3.0417(5)
Zn−Q1 × 2	2.313(2)	2.4315(6)	2.6348(9)	2.636(1)
Zn−Q2 × 2	2.419(1)	2.5270(6)	2.716(1)	2.722(1)
Yb···Zn	3.3314(3)	3.4301(3)	3.6446(4)	3.6629(5)

SHELXL of the SHELXTL suite of programs.[16] Each final refinement included anisotropic displacement parameters and a secondary extinction correction. The program STRUCTURE TIDY[17] was used to standardize the positional parameters. Additional crystallographic details and selected interatomic distances are given in Tables 2−5 and in Supporting Information.

Magnetic Susceptibility Measurements. These were made with a Quantum Design SQUID magnetometer (MPMS5 Quantum Design) for $CsLnMnSe_3$ (Ln = Gd, Tb, Dy, Ho, Er, Tm, and Yb). Impurities were removed from the samples on the basis of crystal color and morphology. The composition of each sample was verified by EDX or X-ray powder diffraction measurements. All samples were ground and loaded into gelatin capsules. Zero-field cooled (ZFC) susceptibility data were collected on the samples between 5 and 300 K. Additionally, field-cooled (FC) susceptibility data were collected on $CsYbMnSe_3$, $CsYbZnS_3$, $RbYbZnSe_3$, and $CsYbZnSe_3$ from 5 to 300 K. The applied field varied from 100 to 500 G. All measurements were corrected for core diamagnetism.[18] The susceptibility data in the temperature range 100−300 K were fit by a least-squares method to the Curie−Weiss equation $\chi = C/(T-\theta_p)$, where C is the Curie constant and θ_p is the Weiss constant. The effective magnetic moment (μ_{eff}) was calculated from the equation $\mu_{eff} = (7.997C)^{1/2}\,\mu_B$.[19] The resulting values for C, θ_p, and μ_{eff} are summarized in Table 6. The magnetic properties of $CsYMnSe_3$ and $CsSmMnSe_3$ were not examined in detail owing to contamination with magnetic Mn/Se binary compounds. The contaminants differed in color from the desired products and crystallized on the faces of the larger quaternary materials. Although the contaminants were clearly visible, they could not be removed easily. We do not know why these two compounds are more susceptible to surface contamination than the other materials.

Table 6. Magnetic Properties of $ALnMQ_3$

	mass (mg)	C (emu K mol^{-1})	θ_p (K)	μ_{eff} (μ_B), obsd	μ_{eff} (μ_B), theory[a]
$CsGdMnSe_3$	10.8	12.39(1)	−70.1(5)	9.96(2)	9.90
$CsTbMnSe_3$	48.0	15.25(6)	−44.0(5)	11.04(6)	11.38
$CsDyMnSe_3$	14.3	17.87(2)	−30.6(4)	11.96(3)	12.14
$CsHoMnSe_3$	8.6	18.71(5)	−37.4(9)	12.23(7)	12.14
$CsErMnSe_3$	64.3	15.11(2)	−44.6(6)	10.99(5)	11.19
$CsTmMnSe_3$	20.8	9.40(1)	−61.3(2)	8.67(2)	9.61
$CsYbMnSe_3$	6.7	5.83(3)	−89.9(4)	6.83(2)	7.46
$CsYbZnS_3$	14.2	2.78(3)	−26.6(6)	4.72(1)	4.54
$RbYbZnSe_3$	25.0	2.89(5)	−22.3(2)	4.81(5)	4.54
$CsYbZnSe_3$	46.5	2.69(1)	−50.2(2)	4.64(2)	4.54

[a] Reference 44.

Neutron Diffraction Measurements. Time-of-flight neutron powder diffraction data were collected on a 2.2 g sample of $CsYbZnSe_3$ on the Special Environment Powder Diffractometer (SEPD)[20] at the Intense Pulsed Neutron Source (IPNS) at Argonne National Laboratory. Diffraction data were collected at eight

(17) Gelato, L. M.; Parthé, E. *J. Appl. Crystallogr.* **1987**, *20*, 139−143.
(18) *Theory and Applications of Molecular Diamagnetism*; Mulay, L. N., Boudreaux, E. A., Eds.; Wiley-Interscience: New York, 1976.
(19) O'Connor, C. J. *Prog. Inorg. Chem.* **1982**, *29*, 203−283.

Table 7. Refined Structural Parameters of $CsYbZnSe_3$ from the Rietveld Analysis of the Neutron Diffraction Data[a]

param	4 K	295 K
a (Å)	4.07852(5)	4.0937(1)
b (Å)	15.7299(2)	15.8617(3)
c (Å)	10.7947(1)	10.8175(1)
V (Å^3)	692.53(2)	702.41(2)
R_{exp}[b]	0.0361	0.0369
R_{wp}[c]	0.0471	0.0439

[a] For the structure, $Z = 4$ and space group = $Cmcm$. [b] $R_{exp} = (n - m)^{1/2}[\sum_i w_i y(\text{obsd})_i^2]^{-1/2}$. [c] $R_{wp} = \{\sum_i w_i[y(\text{obsd})_i - y(\text{calc})_i]^2\}^{1/2}/\{\sum_i w_i y(\text{obsd})_i^2\}^{1/2}$, where n = number of data points; m = number of refined parameters; $w_i = 1/y(\text{obsd})_i$; $y(\text{obsd})_i$ = observed intensity at step i (including background); $y(\text{calc})_i$ = calculated intensity at step i (including background).

different temperatures in the range from 4 to 295 K. Cooling was achieved with a Leybold closed-cycle helium refrigerator. Diffraction data were analyzed by the Rietveld refinement method with the GSAS (EXPGUI) suite of programs.[21,22] Refined structural parameters at 4 and 295 K from the Rietveld analysis are presented in Table 7, and atomic coordinates may be found in Supporting Information.

Optical Measurements. Absorption measurements were performed on single crystals of $CsYbMnSe_3$, $CsYbZnS_3$, and $RbYbZnSe_3$ with the use of an Ocean Optics model S2000 spectrometer over the range 400 nm (3.10 eV) to 800 nm (1.55 eV) at 293 K. The spectrometer was fiber optically coupled to a Nikon TE300 inverted microscope. White light originated from the TE300 lamp and passed through a polarizer before reaching the sample. Face-indexed single crystals were positioned at the focal point above the 20× objective with the use of a goniometer mounted on translation stages (Line Tool Company). The light transmitted through the crystal was then spatially filtered before being focused into the 400 μm core diameter fiber coupled to the spectrometer. Fine alignment of the microscope assembly was achieved by maximizing the transmission of the lamp profile. The extinction spectra of both the (010) and (001) crystal planes (light perpendicular to the *ac* and *ab* crystal planes, respectively) for $CsYbMnSe_3$ were recorded. Owing to the small size of the $CsYbZnS_3$ and $RbYbZnSe_3$ crystals only spectra of the (010) crystal faces were recorded. Optical band gaps were calculated by the linear regression techniques described previously.[12,13] The absorption edges of the remaining $CsLnMnSe_3$ compounds were obscured by intense Mn-based d−d transitions that prohibited the calculation of the optical band gaps. Similar transitions were observed in the optical spectra of the $K_2Cd_{3(1-x)}Mn_{3x}S_4$.[23]

Results and Discussion

Syntheses. The compounds $CsLnMnSe_3$ (Ln = Sm, Gd, Tb, Dy, Ho, Er, Tm, Yb, Y) as well as $CsYbZnS_3$ and $RbYbZnSe_3$ were obtained in at least 80% yield. In contrast, only a few crystals of $RbYbZnTe_3$ and $CsYbZnTe_3$ were obtained. No Eu compounds could be synthesized, presumably because of the propensity of Eu to adopt the formal oxidation state 2+ in chalcogenide systems.

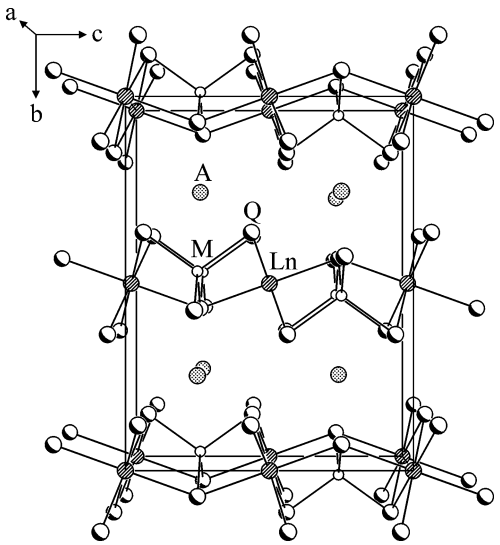

Figure 1. Unit cell of $ALnMQ_3$ viewed down [100]. The A−Q bonds have been removed for clarity.

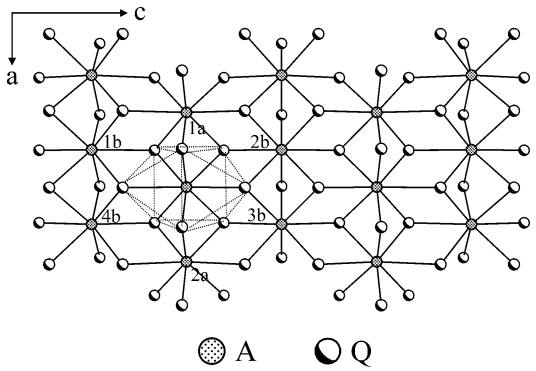

Figure 2. $^2_\infty[LnMq_3]$ layer viewed down [010].

In keeping with the $CsLnZnSe_3$ materials,[12] the $CsLnMnSe_3$ compounds were not obtained with the lighter (and hence larger) rare-earth elements (Table 1). In contrast, the $CsLnMSe_3$ (M = Cd, Hg) compounds[13] were not obtained with the heavier rare-earth elements. It is clear that in these $ALnMQ_3$ compounds as the atomic radius of the transition metal increases so must the radius of the rare earth in order to maintain the anionic framework of edge-sharing MQ_4 tetrahedra and LnQ_6 octahedra and hence the stability of the structure.

Structure Determinations. The structure of the isostructural $ALnMQ_3$ compounds, which is of the $KZrCuS_3$ structure type,[14] is illustrated in Figure 1. It is composed of two-dimensional $^2_\infty[LnMQ_3]$ layers that stack perpendicular to [010] and are separated by A atoms. The A atoms are coordinated to eight Q atoms in a bicapped trigonal prismatic arrangement. Figure 2 illustrates that each AQ_8 prism has two face-sharing neighbors (labeled 1a and 2a) and four edge-sharing ones (labeled 1b−4b) to form a $^2_\infty[AQ_3]$ layer. The Ln atoms are coordinated to a slightly distorted octahedron of six Q atoms, whereas the M atoms are coordinated to a distorted tetrahedron of four Q atoms (Tables 3 and 5). The $^2_4[LnMQ_3]$ layer is constructed from chains of edge-sharing LnQ_6 octahedra and chains of vertex-sharing MQ_4 tetrahedra, as shown in Figure 3. Each tetrahedron in the $^1_\infty[MQ_3]$ chain

(20) Jorgensen, J. D.; Faber, J., Jr.; Carpenter, J. M.; Crawford, R. K.; Haumann, J. R.; Hitterman, R. L.; Kleb, R.; Ostrowski, G. E.; Rotella, F. J.; Worlton, T. G. *J. Appl. Crystallogr.* **1989**, *22*, 321−333.
(21) Larson, A. C.; Von Dreele, R. B. Los Alamos National Laboratory, Los Alamos, NM, LAUR 86-748, 1994.
(22) Toby, B. H. *J. Appl. Crystallogr.* **2001**, *34*, 210−213.
(23) Axtell, E. A., III; Hanko, J.; Cowen, J. A.; Kanatzidis, M. G. *Chem. Mater.* **2001**, *13*, 2850−2863.

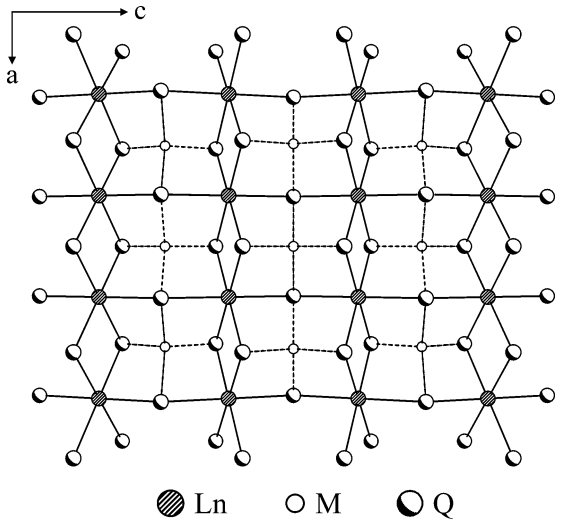

Figure 3. $^{2}_{\infty}$[$LnMQ_3$] layer viewed down [010].

Table 8. Bond Ranges (Å) in the Present $ALnMQ_3$ Compounds and in the Literature

bond	$ALnMQ_3$ bond range	reported bond range	ref
Rb−Se	3.4299(8)−3.7833(6)	3.4989(9) in $RbTh_2Se_6$	45
Rb−Te	3.636(1)−4.0116(9)	3.685(4)−3.866(3) in $RbHgSbTe_3$	46
Cs−S	3.486(2)−3.726(2)	3.532(3)−3.861(2) in $Cs_2Au_2Cd_2S_4$	47
Cs−Se	3.5926(8)−3.9283(7)	3.4281(8)−3.9527(3) in $CsSm_2CuSe_4$	48
Cs−Te	3.790(1)−4.066(1)	3.817(4)−3.929(4) in $CsTh_2Te_6$	49
Sm−Se	2.9206(4)−2.9325(5)	2.8595(4)−3.0086(3) in $CsSm_2CuSe_4$	48
Gd−Se	2.9058(5)−2.9121(5)	2.887(1)−2.928(1) in $BaGdAuSe_3$	26
Tb−Se	2.8896(3)−2.9009(3)	2.8509(6)−2.9240(6) in $CsTb_2Ag_3Se_5$	48
Dy−Se	2.8763(4)−2.8928(3)	2.822(1)−2.9385(8) in $RbDy_2CuSe_4$	50
Y−Se	2.8773(3)−2.8893(3)	2.879(1)−2.910(1) in $BaYAgSe_3$	25
Ho−Se	2.8710(5)−2.8845(6)	2.839(1) in $CdHo_2Se_4$	51
Er−Se	2.8604(4)−2.8729(3)	2.770(2)−2.939(2) in $CsEr_3Se_5$	52
Tm−Se	2.8498(4)−2.8690(4)	2.812(1) in $CdTm_2Se_4$	51
Yb−S	2.7017(9)−2.7237(6)	2.677(2)−2.694(2) in $CaYbInS_4$	53
Yb−Se	2.8177(4)−2.8659(5)	2.752(3)−2.934(2) in $Rb_3Yb_7Se_{12}$	52
Yb−Te	3.0264(4)−3.0501(4)	none reported	
Mn−Se	2.4996(8)−2.5898(7)	2.541(7)−2.579(9) in $Rb_2Mn_3Se_4$	39
Zn−S	2.313(2)−2.419(1)	2.294(9)−2.388(9) in Tm_2ZnS_4	54
Zn−Se	2.4315(6)−2.5270(6)	2.439(1) in $ZnGa_{0.4}Cr_{1.6}Se_4$	55
Zn−Te	2.6348(9)−2.722(1)	2.6819(5) in $KCuZnTe_2$	56

shares edges with four LnQ_6 octahedra to form the $^{2}_{\infty}$[$LnMQ_3$] layers.

In the present materials all of the bond lengths are normal (Tables 3 and 5) and are consistent with previously reported values (Table 8). Additionally, those bonds involving Ln reflect the lanthanide contraction. Because there are no Q−Q bonds in the structure of $ALnMQ_3$, the formal oxidation states of A/Ln/M/Q are 1+/3+/2+/2−.

A number of alkali-metal or alkaline earth/rare-earth or U/transition-metal/chalcogenides possess the 1/1/1/3 stoichiometry. These materials predominantly crystallize in the $KZrCuS_3$[14] and Eu_2CuS_3[24] structure types. In addition to the present and earlier compounds of this series,[12,13] $ALnMQ_3$ materials that adopt the $KZrCuS_3$ structure include $KZrCuQ_3$ (Q = Se, Te),[14] $BaErCuS_3$,[25] $BaYAgSe_3$,[25] $BaGdAuSe_3$,[26] $BaYCuTe_3$,[26] $BaYAgTe_3$,[26] $BaDyCuTe_3$,[27] $BaGdCuSe_3$,[28] $CsUCuTe_3$,[29] $KUCuSe_3$,[30] $CsCeCuS_3$,[30] and $TlZrCuTe_3$.[31] In contrast, the Eu_2CuS_3 structure (Figure 4) consists of $Eu^{3+}S_6$ octahedra, $Eu^{2+}S_7$ monocapped trigonal prisms, and CuS_4 tetrahedra. The EuS_6 octahedra and CuS_4 tetrahedra share vertices to form $^{2}_{\infty}$[$EuCuS_3$] layers that stack perpendicular to the [001]. These layers are separated by layers of EuS_7 trigonal prisms. β-$BaLaCuSe_3$[32] and $BaLaCuTe_3$[26] crystallize in the Eu_2CuS_3 structure with La^{3+} in place of Eu^{3+} and Ba^{2+} in place of Eu^{2+}. The structure of Eu_2CuS_3 (space group *Pnma*) is very similar to that of $KZrCuS_3$ (space group *Cmcm*). The structural differences are caused by the relative sizes of the chalcogen and alkali-metal or alkaline-earth atoms. The decreased cationic radius of Eu^{2+} (1.20 Å) in comparison with Rb^+ (1.61 Å) and Cs^+ (1.74 Å)[33] leads to the decrease in coordination numbers. Moreover, the EuS_6 octahedra and CuS_4 tetrahedra of Eu_2CuS_3 are more distorted and possess lower site symmetries than do the LnQ_6 octahedra and MQ_4 tetrahedra of the $ALnMQ_3$ compounds that have the $KZrCuS_3$ structure type. There are more than 60 known $ALnMQ_3$ compounds isostructural with $KZrCuS_3$, far more than those isostructural with Eu_2CuS_3. This is a clear indication of the stability and robustness of the present structure.

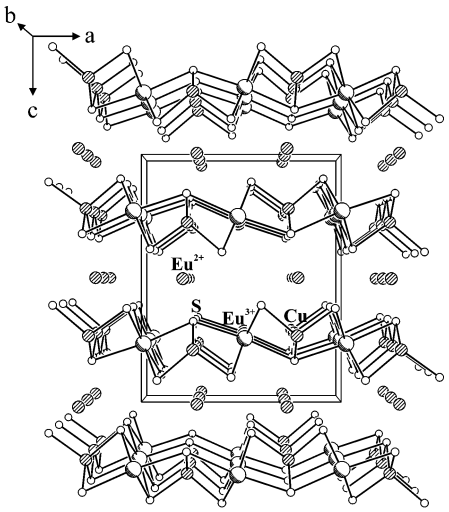

Figure 4. Unit cell of Eu_2CuS_3 viewed down [010]. The Eu^{2+}−S bonds were removed for clarity.

Magnetic Susceptibility Measurements. All of the materials, excluding those containing Yb, are paramagnetic over the temperature range measured. A number of the

(24) Lemoine, P.; Carré, D.; Guittard, M. *Acta Crystallogr. Sect. C: Cryst. Struct. Commun.* **1986**, *42*, 390−391.
(25) Wu, P.; Christuk, A. E.; Ibers, J. A. *J. Solid State Chem.* **1994**, *110*, 337−344.
(26) Yang, Y.; Ibers, J. A. *J. Solid State Chem.* **1999**, *147*, 366−371.
(27) Huang, F. Q.; Choe, W.; Lee, S.; Chu, J. S. *Chem. Mater.* **1998**, *10*, 1320−1326.
(28) Huang, F. Q.; Mitchell, K.; Ibers, J. A. *Inorg. Chem.* **2001**, *40*, 5123−5126.
(29) Cody, J. A.; Ibers, J. A. *Inorg. Chem.* **1995**, *34*, 3165−3172.
(30) Sutorik, A. C.; Albritton-Thomas, J.; Hogan, T.; Kannewurf, C. R.; Kanatzidis, M. G. *Chem. Mater.* **1996**, *8*, 751−761.
(31) Pell, M. A.; Ibers, J. A. *J. Alloys Compd.* **1996**, *240*, 37−41.
(32) Christuk, A. E.; Wu, P.; Ibers, J. A. *J. Solid State Chem.* **1994**, *110*, 330−336.
(33) Shannon, R. D. *Acta Crystallogr. Sect. A: Cryst. Phys. Diffr. Theor. Gen. Crystallogr.* **1976**, *32*, 751−767.

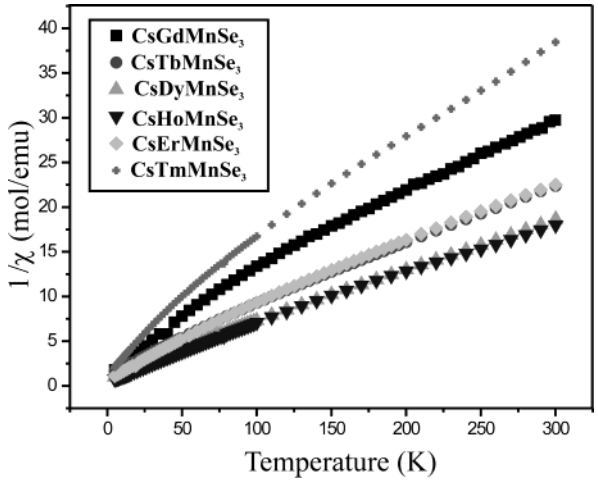

Figure 5. Plot of the inverse molar susceptibility ($1/\chi$) versus T for $CsLnMnSe_3$.

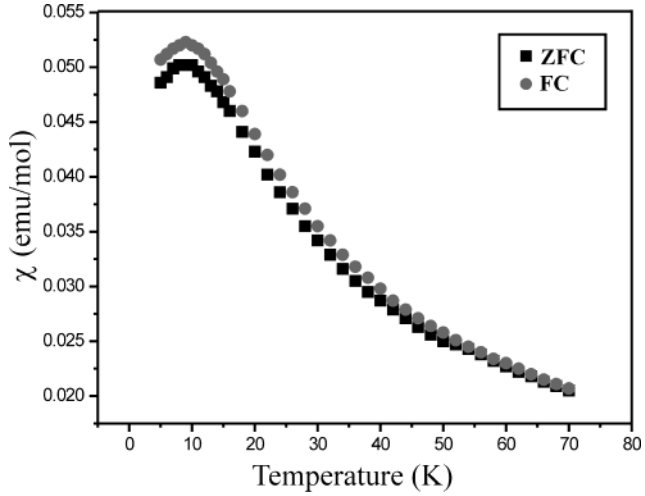

Figure 6. Plot of the molar susceptibility (χ) vs T for $CsYbZnSe_3$.

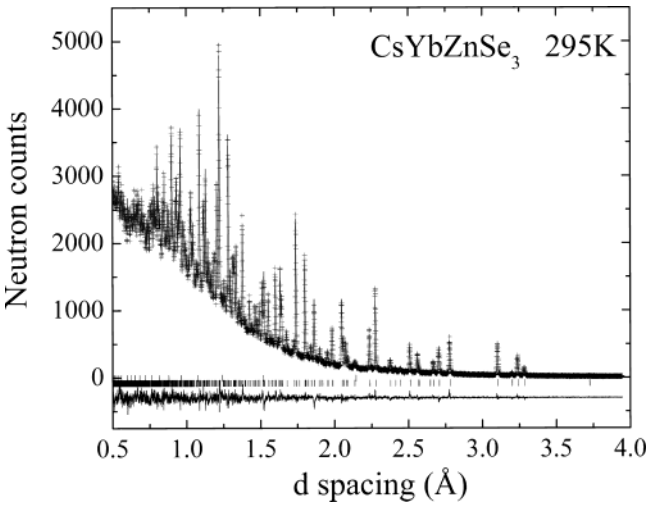

Figure 7. Time-of-flight neutron powder diffraction data (+), and best-fit Rietveld refinement profile (−) and their difference (at the bottom), for $CsYbZnSe_3$ at 295 K. Tick marks indicate the Bragg positions.

compounds deviate from ideal Curie−Weiss behavior below 100 K (Figure 5) as a result of crystal-field effects.[34] Table 6 lists the values of C, θ_p, and μ_{eff} for the paramagnetic materials. The large negative values of θ_p indicate that there is a substantial degree of local antiferromagnetic coupling involving both the Ln^{3+} and Mn^{2+} magnetic cations. Furthermore, the value of μ_{eff} for $CsTmMnSe_3$ is significantly smaller than the theoretical value calculated for Tm^{3+} and Mn^{2+}. This presumably arises from Mn because the electrons of the 4f shell of Tm lie deep inside the ion, within the 5s and 5p shells, whereas the 3d electrons responsible for the magnetic behavior of Mn lie in the outermost shell. In addition to $CsTmMnSe_3$, there are a number of paramagnetic compounds containing Mn^{2+} cations that possess reduced experimental μ_{eff} values. Examples include Ba_2MnQ_3 (Q = S, Se, Te),[35,36] $Na_2Mn_2S_3$,[37] $Cs_2Mn_2S_3$,[38] and $A_2Mn_3Se_4$ (Rb, Cs).[39] Crystal field effects, in addition to magnetic coupling, may play a role in lowering the μ_{eff} values.

A plot of the molar susceptibility χ versus T for $CsYbZnSe_3$ is displayed in Figure 6; magnetic data for $CsYbMnSe_3$, $CsYbZnS_3$, and $RbYbZnSe_3$ lead to very similar plots. Each has a weak cusp centered at approximately 10 K and displays pronounced differences between FC and ZFC data. The calculated μ_{eff} for $CsYbMnSe_3$, as also for $CsTmMnSe_3$, is smaller than the theoretical value. It is interesting that the Yb-containing compounds $CsYbZnS_3$, $RbYbZnSe_3$, $CsYbMnSe_3$, and $CsYbZnSe_3$ possess the shortest Ln···M distances (Tables 3 and 5) and are the only compounds that exhibit transitions. This simple chemical change of the Ln atom causes a significant change in the magnetic properties of these compounds and highlights the fact that the magnetic properties of the $ALnMQ_3$ (M ≠ Cu, Ag, Au) compounds are more interesting than those of the coinage metals. Additional and possibly useful magnetic phenomena may be observed with further chemical substitution, for example with M = Fe.

Neutron Diffraction Measurements. The room-temperature neutron powder diffraction pattern of $CsYbZnSe_3$ is displayed in Figure 7. Additional structural information is summarized in Table 7 and in Supporting Information. The structure derived from these neutron powder data is in good agreement with that obtained from single-crystal X-ray data.[12] At 4 K the neutron diffraction pattern of $CsYbZnSe_3$ exhibits no reflections in addition to those observed at room temperature. An increase in intensity of selected low-Q reflections, as is expected from a ferromagnetic ordering, is not observed. Therefore, there is no evidence of long-range (>1000 Å) magnetic ordering.

The normalized lattice parameters (l/l_0; $l = a$, b, or c of this *Cmcm* structure) versus temperature, obtained from the neutron diffraction data, are shown in Figure 8. The thermal expansion can be nicely modeled with the Grüneisen model

(34) Cascales, C.; Sáez-Puche, R.; Porcher, P. *J. Solid State Chem.* **1995**, *114*, 52−56.
(35) Grey, I. E.; Steinfink, H. *Inorg. Chem.* **1971**, *10*, 691−696.
(36) Greaney, M. A.; Ramanujachary, K. V.; Teweldemedhin, Z.; Greenblatt, M. *J. Solid State Chem.* **1993**, *107*, 554−562.
(37) Klepp, K.; Böttcher, P.; Bronger, W. *J. Solid State Chem.* **1983**, *47*, 301−306.
(38) Bronger, W.; Hendriks, U.; Müller, P. *Z. Anorg. Allg. Chem.* **1988**, *559*, 95−105.
(39) Bronger, W.; Hardtdegen, H.; Kanert, M.; Müller, P.; Schmitz, D. *Z. Anorg. Allg. Chem.* **1996**, *622*, 313−318.

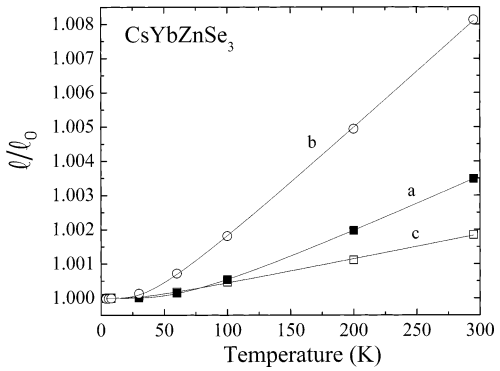

Figure 8. Normalized lattice parameters of $CsYbZnSe_3$. Lines are best fit of the data to the Grüneisen model for a single phonon. l_0 is the lattice parameter at 0 K, determined from the fit.

for a single phonon:[40] $\ln(l/l_0) = \alpha T_E(\exp(T_E/T) - 1)^{-1}$, where l is the lattice parameter (a, b, or c), l_0 is its value at $T = 0$, T_E is the Einstein temperature, T is the temperature, and α is a scaling coefficient. The data of Figure 8 have been fit with this relation for a, b, and c independently, resulting in T_E values of 98(3) K, 46(3) K, and 55(1) K, respectively. The thermal expansion along the b axis is more than twice as large as the thermal expansion along either a or c. This effect is expected in the layered structure of $CsYbZnSe_3$, where the bond interactions perpendicular to the $^2_\infty[YbZnSe_3]$ layers are the weakest. The values of the lattice constants at $T = 153$ K, calculated from this fit to the neutron diffraction powder data, of 4.0837(1), 15.7843(3), and 10.8033(1) Å for a, b, and c, respectively, are in excellent agreement with the values of 4.0853(4), 15.7866(15), and 10.8068(10) Å obtained in the single-crystal X-ray study.[12]

Magnetic Nature of $CsYbZnSe_3$. Because the neutron diffraction results indicate that there is neither long-range magnetic order nor any structural change in $CsYbZnSe_3$, the compound is not an antiferromagnet as we originally thought.[12] Although the differences in FC and ZFC magnetic data are characteristic of a spin glass, ac magnetic measurements exclude this, because there is no dependence of the transition at approximately 10 K on frequency between 10 and 2000 Hz.[41] Thus $CsYbZnSe_3$, and presumably the other Yb-containing compounds above, namely $CsYbMnSe_3$, $CsYbZnS_3$, and $RbYbZnSe_3$, join $BaLa_2FeS_5$[42] and $K_2Mn_3S_4$[23] as metal chalcogenides whose magnetic properties are difficult to explain.

Optical Measurements. A summary of the single-crystal absorption measurements for the $ALnMQ_3$ compounds examined is presented in Table 9; spectral and band gap information is available in Figure 9 for $RbYbZnSe_3$. The colors of these materials are consistent with the derived band gaps. Although the colors of the Zn, Cd, and Hg materials vary,[12,13] all of the Mn materials are red-brown, a common color among Mn-containing chalcogenides.[23,43]

Table 9. Face-Dependent Optical Band Gaps for Selected $ALnMQ_3$ Materials

compd	color	(010) face[a] (eV)	(001) face[b] (eV)
$CsYbMnSe_3$	red/brown	1.60	1.59
$CsYbZnS_3$	yellow	2.61	
$RbYbZnSe_3$	red	2.07	
$CsYbZnSe_3$[c]	red	2.10	1.97

[a] Light in the [010] direction. [b] Light in the [001] direction. [c] Reference 13.

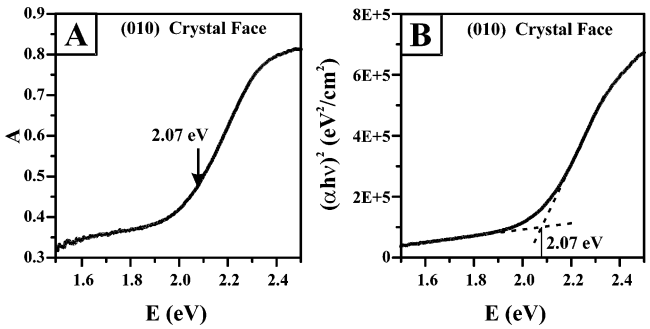

Figure 9. Optical absorption spectra and band gap calculation for a $RbYbZnSe_3$ crystal: (A) absorption spectra of (010) crystal face and (B) plot of absorption data for the (010) face.

Previous density functional theory calculations on the $CsYMSe_3$ (M = Zn, Cd, Hg) materials indicated these compounds are direct band gap semiconductors and that the highest occupied molecular orbitals (HOMO) are primarily Se1 (4p) and Se2 (4p) in character, whereas the lowest unoccupied molecular orbitals (LUMOs) have contributions from M (ns and np), Y (4d), and Se (4s and 4p).[13] These findings provide a guide for manipulating the optical band gaps of the $ALnMQ_3$ materials. Chalcogen substitution should provide the largest change in the optical properties because the Q atoms contribute to both the HOMO and LUMO. Substitution of the M and Ln atoms should also affect the optical band gaps of the compounds but not as greatly as chalcogen substitution. Experimentally, the substitution of Se for S in $CsYbZnS_3$ results in a change in the optical band gap energy of 0.51 eV. The substitution of Zn for Mn in $CsYbMnSe_3$ results in a similar change (0.5 eV). But the change in energy owing to chalcogen substitution is in fact significantly larger because $RbYbZnTe_3$ and $CsYbZnTe_3$ are black in color. Unfortunately, their color prevented the band gaps of these materials from being measured. In

(40) Wang, K.; Reeber, R. R. *Appl. Phys. Lett.* **2000**, *76*, 2203−2204.
(41) Tkachuk, A. V.; Mar, A. Unpublished results.
(42) Wakeshima, M.; Ino, K.; Hinatsu, Y. *Solid State Commun.* **2001**, *120*, 145−148.
(43) Kim, J.; Hughbanks, T. *J. Solid State Chem.* **1999**, *146*, 217−225.
(44) Kittel, C. *Introduction to Solid State Physics*, 6th ed.; Wiley: New York, 1986.
(45) Choi, K.-S.; Patschke, R.; Billinge, S. J. L.; Waner, M. J.; Dantus, M.; Kanatzidis, M. G. *J. Am. Chem. Soc.* **1998**, *120*, 10706−10714.
(46) Li, J.; Chen, Z.; Wang, X.; Proserpio, D. M. *J. Alloys Compd.* **1997**, *262*−*263*, 28−33.
(47) Axtell, E. A., III; Kanatzidis, M. G. *Chem. Eur. J.* **1998**, *4*, 2435−2441.
(48) Huang, F. Q.; Ibers, J. A. *J. Solid State Chem.* **2001**, *158*, 299−306.
(49) Cody, J. A.; Ibers, J. A. *Inorg. Chem.* **1996**, *35*, 3836−3838.
(50) Huang, F. Q.; Ibers, J. A. *J. Solid State Chem.* **2000**, *151*, 317−322.
(51) Range, K.-J.; Eglmeier, C. *J. Alloys Compd.* **1991**, *176*, L13−L16.
(52) Kim, S.-J.; Park, S.-J.; Yun, H.; Do, J. *Inorg. Chem.* **1996**, *35*, 5283−5289.
(53) Carpenter, J. D.; Hwu, S.-J. *Chem. Mater.* **1992**, *4*, 1368−1372.
(54) Lemoine, P.; Tomas, A.; Vovan, T.; Guittard, M. *Acta Crystallogr. Sect. C: Cryst. Struct. Commun.* **1990**, *46*, 365−368.
(55) Okonska-Kozlowska, I.; Malicka, E.; Waskowska, A.; Mydlarz, T. *J. Solid State Chem.* **1999**, *148*, 215−219.
(56) Heulings, H. R., IV; Li, J.; Proserpio, D. M. *Main Group Met. Chem.* **1998**, *21*, 225−229.

contrast, changing the crystal orientation leads to a smaller change in $CsYbZnSe_3$ (0.13 eV) and to virtually no change in $CsYbMnSe_3$.[13] We do not know why some $ALnMQ_3$ materials exhibit larger band gap changes with crystal orientation than others. Last, in agreement with the theoretical calculations, change of the alkali metal ($RbYbZnSe_3$ versus $CsYbZnSe_3$ in Table 9) has essentially no effect on the optical band gap. These findings provide a guideline for the manipulation of the optical properties of future member of this family of compounds and related materials.

Acknowledgment. We are indebted to Dr. Andriy V. Tkachuk and Prof. Arthur Mar of the University of Alberta for the ac susceptibility measurements. This research was supported by National Science Foundation Grant DMR00-96676, a Ford Predoctoral Fellowship to K.M., and a Northwestern University Presidential Fellowship to C.L.H. At Argonne National Laboratory this work was supported by the U.S. Department of Energy—Office of Science under Contract W-31-109-ENG-38. Use was made of the Central Facilities supported by the MRSEC program of the National Science Foundation (DMR00-76097) at the Materials Research Center of Northwestern University.

Supporting Information Available: Crystallographic files in CIF format for $CsLnMnSe_3$ (Ln = Sm, Gd, Tb, Dy, Ho, Er, Tm, Yb, Y), $CsYbZnS_3$, $CsYbZnTe_3$, $RbYbZnSe_3$, and $RbYbZnTe_3$ and Table 10, a tabulation of atomic coordinates for $CsYbZnSe_3$, as derived from the Rietveld analysis of 4 and 295 K neutron diffraction powder data. This material is available free of charge via the Internet at http://pubs.acs.org.

IC030232+